Nonlinear Mechanical Effects in Silicon Longitudinal Mode Beam Resonators

Ville Kaajakari, Tomi Mattila, Antti Lipsanen, and Aarne Oja

***Abstract*— The fundamental nonlinear mechanical effects in micromachined single-crystal silicon resonators are investigated. Longitudinal mode beam resonators are chosen for the analysis due to their simple geometry and high quality factor ($Q > 100\,000$). Analytical model for the resonator is developed in terms of nonlinear engineering Young's modulus that incorporates both geometrical and material effects. For comparison with the theory, beam resonators were fabricated in two different crystalline directions. The measured nonlinearity is larger for beams in [110] direction than for beams in [100] direction in agreement with the theoretical prediction. The results provide a quantitative value for the appearance of the material-induced nonlinear effects in single-crystal silicon microresonators.**

***Index Terms*— Bulk acoustic wave devices, Hysteresis, Microresonators, Nonlinear oscillators, Nonlinearities, Resonators**

I. Introduction

Micromechanical oscillators and filters are a potential alternative to the size consuming and costly macroscopic components such as quartz resonators. Silicon resonators are seen as an especially interesting technology due to their compact size and suitability for integration with IC technologies [1]. However, the small size of micromechanical components in comparison to their macroscopic counter parts unavoidably results in a smaller power handling capacity. Thus, for optimal performance, the devices may need to be operated close to the material limits for linear operation. Quantifying these limits is therefore of fundamental significance.

Comparison of different microresonator types has shown that bulk acoustic wave based resonators are capable of orders-of-magnitude higher energy storage density than flexural resonators [2]. Moreover, the measured nonlinear vibrations have been close to the estimated material limits. However, no experimental evidence on the material nonlinearity in silicon resonators have been presented.

In this paper, the nonlinear effects in silicon resonators are quantified theoretically and experimentally for single-crystal silicon longitudinal mode devices. The operation of the longitudinal mode resonators is based on bulk acoustic waves; Consequently, the resonators have been shown to offer high quality factors over 100 000 making them suitable for low noise oscillators [3]. While different resonator geometries, plate resonators in particular [4], offer equally high quality factor and much higher power handling capacity, the one dimensional nature of the beam resonators makes them well suited for the analysis of the fundamental resonator performance limits. By measuring resonators oriented in different crystalline directions, direct evidence on material nonlinearity is obtained.

The paper is organized as follows: First, in Section II, the large deformation theory is used to calculate nonlinear silicon Young's modulus. Due to material effects, the nonlinearity is found to be larger for beams in $[110]$ direction than for beams in $[100]$ direction. In Section III, a lumped equivalent model that includes the nonlinear Young's modulus is developed for the longitudinal mode beam resonator. In Section IV, the theory of nonlinear forced vibrations is applied to the lumped beam resonator model. An analytical expression is given to estimate the resonator vibration amplitude maximum limited by hysteresis. In Section V, the lumped model is compared to simulations based on a continuum model and excellent agreement is obtained. The paper is concluded with Section VI where experimental results on measured nonlinearities are given. The predicted difference between the $[110]$ and $[100]$ direction is verified. In general, the results provide a quantitative value for the onset of the material-induced nonlinear effects in single-crystal silicon microresonators. This is of fundamental importance in determining the microresonator performance.

II. Silicon nonlinearity

Single-crystal silicon is often regarded as a linear material until the fracture point. However, a high quality factor makes microresonators susceptible to nonlinearities and even the small silicon material nonlinearity can become significant. In addition to the material nonlinearity, large deformations also result in geometrical nonlinear effects. As an example, the beam cross sectional area decreases in response to stretching force and the Cauchy stress $\sigma = F/A$ for a given force becomes higher. In this paper, the geometrical and material nonlinear effects are incorporated into nonlinear Young's modulus that is calculated using the large deformation theory and the published values for the silicon third-order stiffness tensor [5].

The nonlinear engineering Young's modulus is defined as

$$Y = \frac{T}{S} = Y_0(1 + Y_1 S + Y_2 S^2), \tag{1}$$

where T is the force divided by the initial undeformed area (first Piola-Kirchoff or engineering stress), $S = \partial u/\partial x$ is the displacement gradient with respect to undeformed coordinates (engineering strain), and Y_1 and Y_2 are the first- and

Address: VTT Technical Research Center of Finland, VTT Information Technology, Tietotie 3, Espoo, FIN-02044 VTT, Finland
Corresponding author: ville.kaajakari@vtt.fi
This is a pre-print of paper published in Sensors and Actuators A: Physical, vol. 120(1), pp. 64-70 , 29 April 2005.
doi:10.1016/j.sna.2004.11.010

TABLE I
CALCULATED NONLINEAR ENGINEERING YOUNG'S MODULUS

	Y_0[GPa]	Y_1	Y_2
Beam ([100])	130	0.65	−4.6
Beam ([110])	170	−2.6	−8.1

second-order corrections to the linear Young's modulus Y_0, respectively. To calculate the linear and nonlinear terms in Equation (1), we start from the Cauchy stress due to a finite deformation. Including the geometrical (area and volume) changes and material stiffness effects, the Cauchy stress is

$$\sigma_{ij}(X) = \frac{\rho_X}{\rho_a}\frac{\partial X_i}{\partial a_k}\frac{\partial X_j}{\partial a_k}(c_{ijkl}\eta_{kl} + c_{ijklmn}\eta_{kl}\eta_{mn}), \quad (2)$$

where X is the particle coordinate at the finite deformation, a is the undeformed state, ρ_X and ρ_a are the deformed and undeformed densities, c_{ijlk} and c_{ijklmn} are the second- and third-order stiffness tensors, and η_{kl} is the Lagrangian strain [6]. For the silicon stiffness tensor, experimentally obtained values (in units of GPa) $c_{11} = 165.64$, $c_{12} = 63.94$, $c_{44} = 79.51$, $c_{111} = -795$, $c_{112} = -445$, $c_{123} = -75$, $c_{144} = 15$, $c_{155} = -310$, $c_{456} = -86$ are used [5]. The third-order elastic coefficients are sufficient to describe elastic waves in silicon at high stress levels (9.2 GPa) and the contribution of fourth order elastic coefficients is negligible [7]. The second-order expansion for Young's modulus (Equation (1)) therefore accurately describes the silicon nonlinearities in microresonators. This is different from quartz where the fourth-order elastic coefficients are significant.

Here, Equation (2) is solved numerically as a function of applied stress. The Cauchy stress is then related to the engineering stress, also known as the first Piola-Kirchoff stress by

$$T_{ii} = \left(\frac{\partial X_i}{\partial a_i}\right)^2 \sigma_{ii}. \quad (3)$$

The engineering strain is given by

$$S_{ii} = \frac{\partial X_i}{\partial a_i} - 1. \quad (4)$$

The nonlinear Young's modulus is obtained by fitting the calculated strain and stress given by Equations (2), (3) and (4) to Equation (1). The obtained values for the Young's modulus in [100] and [110] direction are tabulated in Table I with values in [100] direction agreeing with the published analytical results in [6]. The contribution of the anharmonic stiffness tensor c_{ijklmn} is found to be significant. Accounting only for the geometric effects gives $Y_1 = 1.0$ and $Y_2 = 0.50$ for the beam extension in both [100] and [110] direction. This difference between the geometrical and material effects can be used to experimentally verify the presence of material effects: If only the geometrical effects were significant, no difference in nonlinearity would be observed for resonators in [100] and [110] direction whereas an observed difference indicates material nonlinearity.

III. NONLINEAR BEAM RESONATOR MODEL

The longitudinal mode beam resonator used in this study is shown in Figure 1. The vibration mode is a half wave length

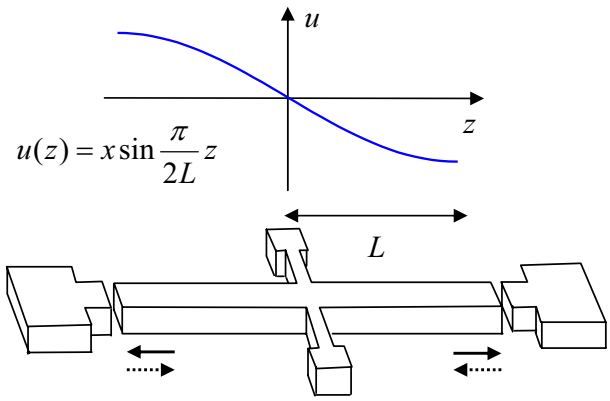

Fig. 1. Schematic of the longitudinal mode beam resonator and the first mode shape

longitudinal mode wave, thus, the device is sometimes referred to a bulk acoustic wave (BAW) resonator [3]. Here a model for the resonator is developed that incorporates the nonlinear Young's modulus calculated in Section II.

The wave equation for a longitudinal displacement u in beams is

$$\rho A\frac{\partial^2 u}{\partial t^2} = \frac{\partial}{\partial z}\left(AY\frac{\partial u}{\partial z}\right), \quad (5)$$

where, ρ is the beam density, A is the beam cross sectional area, and Y is the nonlinear Young's modulus that includes the area and volume changes and the nonlinear material effects [8]. The solution of Equation (5) can be approximated by the linear mode shape

$$u(z,t) = x(t)\sin\pi z/2L, \quad (6)$$

where x is the motion of the beam tip and L is the beam half length [9], [3]. The linear mode shape approximation is justified by numerical simulations in Section V. Substituting Equations (1) and (6) into (5) and integrating over the mode shape leads to

$$\rho AL\frac{\partial^2 x}{\partial t^2} = -\frac{\pi^2}{4}\frac{AY}{L}x\left(1 + \frac{4Y_1}{3L}x + \frac{3\pi^2 Y_2}{16L^2}x^2\right). \quad (7)$$

The effective mass and the nonlinear spring constants can be recognized as

$$\begin{aligned} &m = \rho AL \\ &k(x) = k_0(1 + k_1 x + k_2 x^2) \\ &k_0 = \tfrac{\pi^2}{4}\tfrac{AY}{L}, k_1 = \tfrac{4Y_1}{3L} \text{ and } k_2 = \tfrac{3\pi^2 Y_2}{16L^2}. \end{aligned} \quad (8)$$

Thus, the nonlinear vibrations in a longitudinal mode beam resonator can be modeled as a lumped second order system. The equation of motion for forced beam vibrations is written as

$$m\ddot{x} + \gamma\dot{x} + k(x)x = F_\omega\cos\omega t, \quad (9)$$

where x is the motion of beam tip, γ is the damping coefficient, F_ω is the magnitude of the forcing term at frequency ω, and the mass and spring constant are given by Equation (8). We also define the natural frequency $\omega_0 = \sqrt{k/m}$ and the quality factor $Q = \omega_0 m/\gamma$.

IV. NONLINEAR FORCED VIBRATIONS

The lumped model can be used to analytically characterize the resonator nonlinearities and to estimate the maximum vibration amplitude. Following Landau, the solutions to Equation (9) are searched by the method of successive approximations by assuming a solution of form [10]

$$x(t) = x_0 + x_1 \cos\omega t + x_2 \cos 2\omega t + x_3 \cos 3\omega t + ... \quad (10)$$

The resonance behavior changes in the presence of nonlinear terms and the peak frequency ω_0' is related to the vibration amplitude x_1 by

$$\omega_0' = \omega_0(1 + \kappa x_1^2), \quad (11)$$

where

$$\kappa = \frac{3}{8}k_2 - \frac{5}{12}k_1^2. \quad (12)$$

The time harmonic vibration amplitude near the resonance is then given by

$$x_1 = \frac{F_\omega/m}{\sqrt{(\omega_0'^2 - \omega^2)^2 + (\omega\omega_0'/Q)^2}}. \quad (13)$$

Equations (11), (12) and (13) show that due to either positive or negative k1, the peak frequency always shifts to a lower frequency with an increasing vibration amplitude x_1. Similarly, a negative k_2 results in the peak frequency shifting to a lower frequency, but a positive k_2 results in a higher peak frequency. As indicated by Table I and Equation (8), the k_2:s are negative for both crystalline directions. Due to the combined x_1 and k_2 effects, the resonator peak frequency is always expected to show a shift to a lower frequency.

A useful measure of the maximum vibration amplitude is obtained by calculating the bifurcation point shown in Figure 2(a). At higher excitation levels, the amplitude-frequency relationship is no longer a single valued function and shows hysteresis as illustrated in Figure 2(b). The vibration amplitude at the point of bifurcation is

$$x_b = \frac{1}{\sqrt{\sqrt{3}Q|\kappa|}}. \quad (14)$$

As indicated in Figure 2(a), the critical vibration amplitude (or the greatest vibration amplitude) is slightly higher than the vibration amplitude at the bifurcation point and is given by

$$x_c = \frac{2}{\sqrt{3\sqrt{3}Q|\kappa|}}. \quad (15)$$

As Equation (15) shows, increasing the quality factor *lowers* the critical vibration amplitude x_c as the resonator becomes more susceptible to nonlinearities.

The energy stored in the resonator at the critical vibration amplitude x_c is

$$E_c = \frac{1}{2}k_0 x_c^2 \quad (16)$$

and the drive level defined as power dissipated in the resonator is

$$P_c = \frac{\omega_0 E_c}{Q}. \quad (17)$$

TABLE II
COMPARISON OF 10 MHZ LONGITUDINAL MODE RESONATORS ORIENTED IN [100] AND [110] DIRECTION

Parameter	Symbol	Orientation [100]	Orientation [110]	Units
Resonator height	h	10	10	μm
Resonator width	w	10	10	μm
Resonator half length	L	187	213	μm
Linear spring constant	k_0	172	196	kN/m
	k_1	4.7	-15	10^3
	k_2	-3.9	-3.0	10^8
	κ	1.1	2.1	10^8
Mass	m	43.6	49.7	pkg
Quality factor	Q	1	1	10^5
Critical vibration amplitude	x_c	270	190	nm
Energy at critical amplitude	E_m	6.2	3.6	nJ
Power at critical amplitude	P_m	3.9	2.3	μW
Maximum strain	S_c^{max}	2.3	1.4	10^{-3}

Equations (16) and (17) can be used to compare the power handling capacity of different resonators [2]. Table II shows the critical vibration amplitudes for 10 MHz longitudinal mode beam resonators oriented in [100] and [110] direction. The following is observed:

1) The resonator oriented in [110] direction is about 14% larger than the resonator in [100] direction reflecting the larger linear Young's modulus in [110] direction. Thus, if one were not to account for the nonlinear material effects, the larger size of the [110] resonator would be expected result in a larger power handling capacity.
2) Due to the inclusion of the material effects, the nonlinearity factor κ for the resonator in [110] direction is almost twice of that in [100] direction. The maximum vibration amplitude x_c is correspondingly about 30% smaller.
3) The maximum power handling capacity for the resonator in [110] direction is about half of that in [100] direction. Thus, perhaps surprisingly, the smaller [100] resonator has a higher power handling capacity due to smaller material nonlinearities in comparison to [110] resonator.

The maximum strains at the nonlinear limit can be compared to the estimated fracture strain of $1 \cdot 10^{-2}$ for silicon [11]. The maximum strain in the resonator center at critical vibration amplitude is

$$S_c^{max} = \frac{\pi x_c}{2L}. \quad (18)$$

Thus, as Table II shows, the nonlinearity limit is reached an order-of-magnitude before the fracture.

V. VERIFICATION OF RESONATOR MODEL

To verify the lumped model developed in Section III, the theoretical vibration amplitude given by Equation (13) was compared to simulations with a distributed model [2]. In the distributed model, the continuum is approximated with a chain of four masses and springs. The mass-spring chain model has been implemented as an electrical-equivalent model in the Aplac simulation software. Displacement versus frequency responses to a forced excitation are simulated using the harmonic balance analysis [12], [13]. As the harmonic balance analysis is carried out in the frequency domain, it is computationally

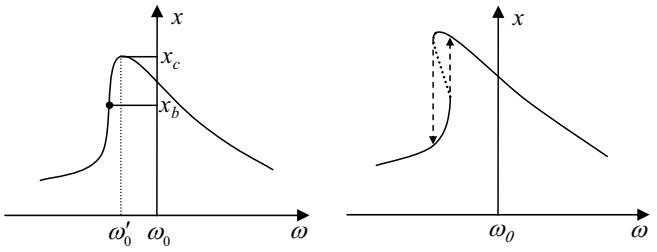

(a) The bifurcation point x_b and critical vibration amplitude x_c used to estimate the maximum vibration amplitude

(b) Unstable region (dotted line) in amplitude-frequency curve resulting in frequency hysteresis (arrows)

Fig. 2. At bifurcation point, the vibration amplitude is not a single valued function leading to frequency hysteresis

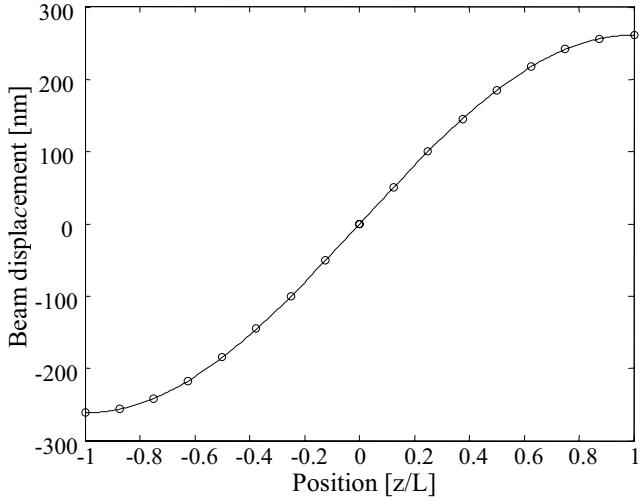

Fig. 3. Simulated mode shape (○) obtained with eight masses and springs at the hysteresis limit and the linear mode shape (-).

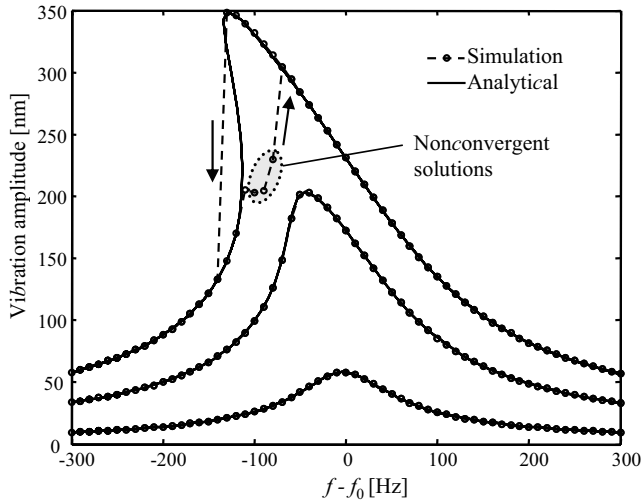

Fig. 4. Analytical and simulated vibration amplitude for a 10 MHz longitudinal mode resonator in [100] direction. The largest excitation level results in hysteresis (sweep direction is indicated with arrows). The grey area indicates nonconvergent solutions.

efficient for systems that have a high quality factor and are thus slow to settle in the time domain (transient) analysis. The convergence of the discretization was verified by repeating the simulations with a model based on eight mass and springs. The difference was less than 1% validating the used discretization.

Figure 3 shows the simulated vibration mode for the eight mass-spring chain at the hysteresis limit and the analytical linear mode shape ($\sin kx$). The relative difference between the nonlinear simulated beam displacements and the linear mode shape is less than $1 \cdot 10^{-3}$ justifying the usage of linear mode shape in Section III. Figure 4 shows a comparison of the analytical lumped model and the simulated distributed model for the 10 MHz longitudinal mode resonator in [100] direction. Excellent agreement is obtained below the bifurcation point. As expected for the negative k_1 and k_2, the peak frequency shifts to a lower frequency as the vibration amplitude increases. At large vibration amplitudes, the solution is not a single valued function and has an unstable region. This is seen as a frequency hysteresis in the simulation. The convergence remains good for the frequency sweep from higher to lower frequency. However, for the sweep from lower to higher frequency, the harmonic-balance solver has trouble finding the solution for the highest excitation level due to hysteresis and resulting sudden jump in vibration amplitude. Thus, it can be concluded that the analytical model and simulations agree but care should be used when simulating vibrations larger than the critical vibration amplitude.

VI. Measured nonlinear vibrations

In order to verify the theoretical results on the nonlinear vibrations, single-crystal silicon beam resonators were fabricated and measured. The beams were etched using DRIE in [100] and [110] directions on SOI wafers. To release the beams, the silicon etching was followed by wet etching of the sacrificial oxide with hydrofluoric acid. To prevent stiction after the release etch and subsequent rinse, CO_2 critical point drying was used. The resonator dimensions were $h = 9$ μm, $w = 10$ μm, and $L = 180$ μm. To eliminate unwanted effects from the capacitive nonlinearity, the resonators were actuated with wide gap (1.5 μm) capacitive transducer [3], [2]. For excitation, symmetric drive configuration shown in Figure 5 was used as it maximizes the vibration amplitude for a given excitation voltage. The measurements were done using a HP4195A network analyzer and the resonance signal was buffered with a JFET preamplifier.

Figure 6 shows transmission curves for a [100] beam. At low excitation level, a linear response is obtained. As the excitation amplitude is increased, the resonance peak shifts to a lower frequency indicating nonlinearity in accordance to Equation (11). Eventually the transmission amplitude - frequency curve shows hysteresis.

To accurately compare the experimental results with the theoretical model, measurement was carried out in two steps. First, a series of transmission curves were measured by varying the bias voltage at a low excitation level. This linear data was used for resonator parameter extraction and for verification of the model. Typical measurement for a beam in [100] direction is shown in Figure 7(a) together with simulated transmission curves. Very good agreement between simulations and

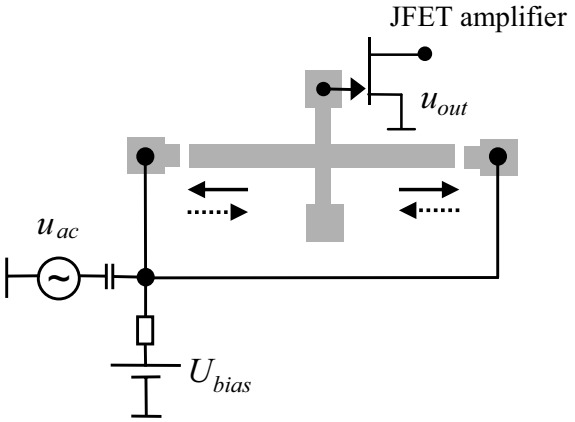

Fig. 5. Schematic of the resonator measurement set-up

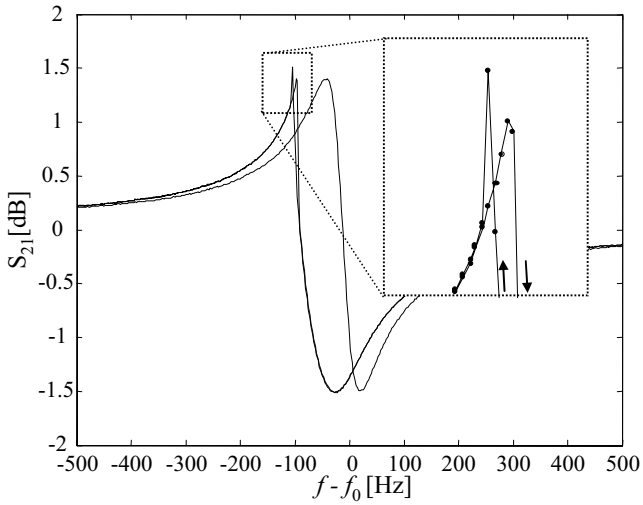

Fig. 6. Measured linear and nonlinear hysteretic response for a [100] beam resonator

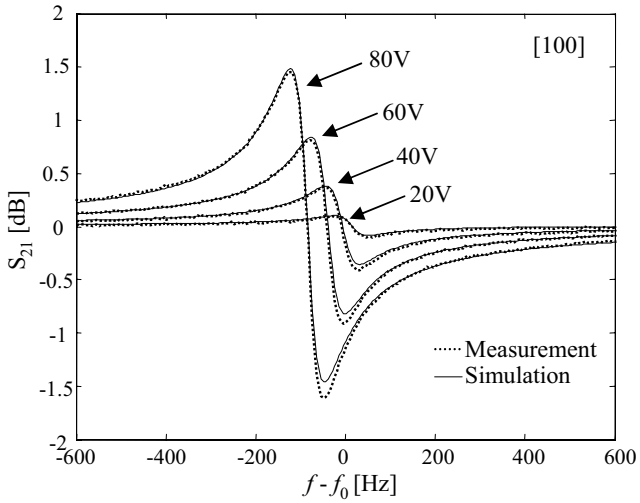

(a) Amplitude-frequency measurement with varying bias voltage ($u_{ac} < 50$ mV)

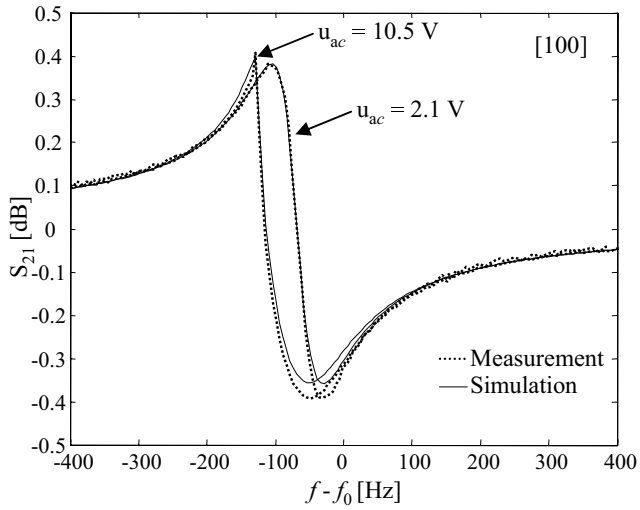

(b) Large amplitude vibration resulting in nonlinear response ($U_{bias} = 40$ V)

Fig. 7. Measured (dotted line) and simulated (solid line) linear and nonlinear transmission curves for a resonator in [100] direction (best fit parameters $Y_1 = 0.4$ and $Y_2 = -2.9$)

measurement is obtained. Next, the driving voltage amplitude was increased to characterize the nonlinearity in the resonator response. Figure 7(b) shows measured and simulated transmission curves with increasing excitation level for the same resonator. Due to the nonlinearity at higher excitation levels, the peak frequency shifts to lower frequency as expected for the negative k_2.

A similar set of data for a beam in [110] direction is shown in Figure 8. The critical observation is that the nonlinearity becomes significant at lower excitation levels for the resonators in [110] direction than for the ones in [100] direction. This is in perfect agreement with the theoretical prediction made in Section IV confirming that the material nonlinearities are significant. If only the geometrical nonlinearities were present, no directional difference in nonlinearity would be expected.

The best fit values for the nonlinear terms in Young's modulus were $Y_1 = 0.4$ and $Y_2 = -2.9$ for the resonators in [100] direction and $Y_1 = -1.7$ and $Y_2 = -5.2$ for the resonators in [110] direction. These are about 40% lower than the predicted theoretical values. One possible explanation is the highly boron doped silicon ($N_B \approx 5 \cdot 10^{18}$ 1/cm^3) used for the microresonators measured in this study. The literature data for the third-order stiffness sensor is for a lightly doped silicon and the effect of doping is not known. Another source of error can be the beam anchoring. The anchors are at the resonator nodal point and thus their effect is minimized. In fact, finite element simulations with Ansys show that the anchor induced frequency shift is less than 0.2% and large deformation analysis did not reveal any difference in nonlinearity between free and anchored beams. Finite anchor effects, however, cannot be completely excluded. Nevertheless, even though a perfect agreement is not obtained, it can be concluded that the measured resonator vibration amplitudes are close to the predicted material limit.

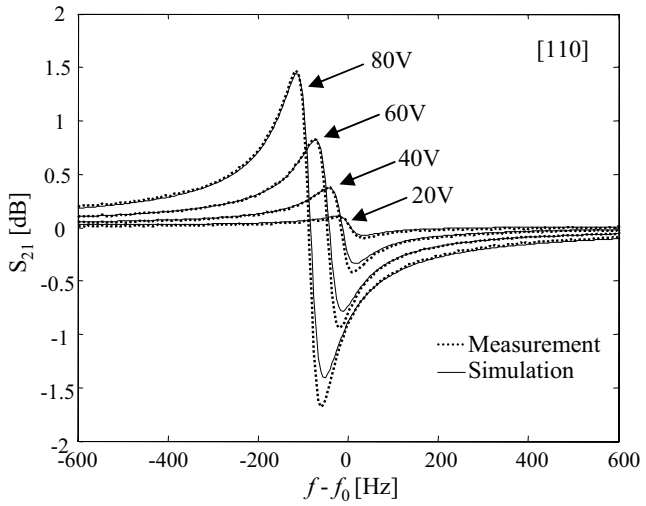

(a) Amplitude-frequency measurement with varying bias voltage ($u_{ac} < 50$ mV)

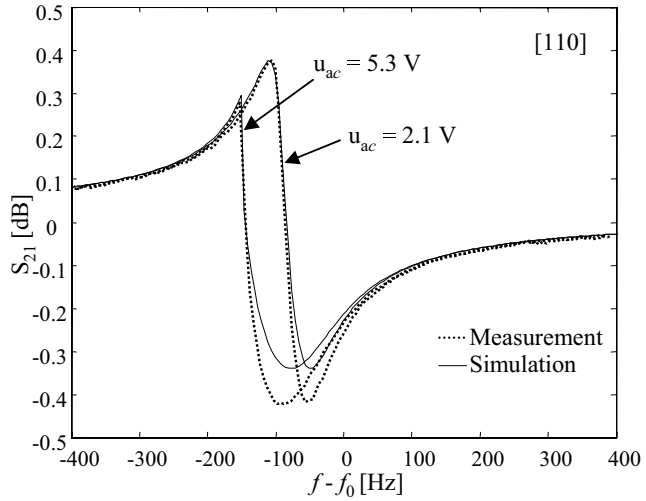

(b) Large amplitude vibration resulting in nonlinear response ($U_{bias} = 40$ V)

Fig. 8. Measured (dotted line) and simulated (solid line) linear and nonlinear transmission curves for a resonator in [110] direction (best fit parameters $Y_1 = -1.7$ and $Y_2 = -5.2$)

VII. Conclusions

Theoretical and experimental methods have shown that the material nonlinearities contribute to the fundamental attainable performance of the high quality factor single-crystal silicon resonators. The predicted difference for resonators aligned in [100] and [110] direction arising from the material nonlinearity was confirmed in the experiments. The longitudinal mode beam resonators were chosen for this study due to their simple geometry, but the obtained results on nonlinear Young's modulus can be generally applied to estimate the single crystal silicon resonator performance limits.

Acknowledgment

We thank A. Alastalo for useful discussions. The financial support from Okmetic, VTI Technologies, and Finnish National Technology Agency is acknowledged.

References

[1] C. T. -C. Nguyen, Frequency-selective MEMS for miniaturized low-power communication devices, IEEE Trans. on Microwave Theory and Techniques 47 (1999) 1486-1503.
[2] V. Kaajakari, T. Mattila, A. Oja, and H. Seppä, Nonlinear limits for single-crystal silicon microresonators, IEEE J. of Microelectromechanical Systems 13 (2004) 715-724.
[3] T. Mattila, J. Kiihamäki, T. Lamminmäki, O. Jaakkola, P. Rantakari, A. Oja, H. Seppä, H. Kattelus, and I. Tittonen, 12 MHz micromechanical bulk acoustic mode oscillator, Sensors and Actuators A 101 (2002) 1-9.
[4] V. Kaajakari, T. Mattila, A. Oja, J. Kiihamäki, and H. Seppä, Square-extensional mode single-crystal silicon micromechanical resonator for low phase noise oscillator applications, IEEE Elect. Dev. Lett. 25 (2004) 173-175.
[5] H. McSkimin and P. Andreatch, Jr., Measurement of third-order moduli of silicon and germanium, J. Appl. Phys. 35 (1964) 3312-3319.
[6] K. Y. Kim and W. Sachse, Nonlinear elastic equation of state of solids subjected to uniaxial homogeneous loading, J. of Material Sci. 35, (2000) 3197-3205.
[7] W. H. Gust and E. B. Royce, Axial yield strengths and two successive phase transition stresses for crystalline silicon, J. Appl. Phys. 42 (1971) 1897-1905.
[8] Karl f. Graff, Wave Motion in Elastic Solids, Dover, New York, 1991.
[9] W. Weaver, Jr., S. Timoshenko, and D. Young, Vibration Problems in Engineering, 5th ed., Wiley, New York, 1990.
[10] L. D. Landau and E. M. Lifshitz, Mechanics, 3rd ed., Butterworth-Heinemann, Oxford, 1999.
[11] C. Wilson and P. Beck, Fracture testing of bulk silicon microcantilever beams subjected to a side load, IEEE J. of Microelectromechanical Systems 5 (1996) 142-150.
[12] T. Veijola and T. Mattila, Modeling of nonlinear micromechanical resonators and their simulation with the harmonic-balance method, Int. J. of RF and Microwave Comput.-Aided Eng. 11 (2001) 310-321.
[13] S. Maas, Nonlinear Microwave and RF Circuits, 2nd Edition, Boston, Artech House, 2003.

Ville Kaajakari received his M.S. and Ph.D. degrees in electrical and computer engineering from University of Wisconsin-Madison in 2001 and 2002, respectively.

He is currently Senior Research Scientist at VTT Information Technology, Finland, where his research interest is RF-MEMS.

Tomi Mattila received his M. Sc. and Dr. Tech. degrees from the Department of Technical Physics at Helsinki University of Technology in 1994 and 1997, respectively.

Since 1999 he has been working as Senior Research Scientist in the MEMS sensors group at VTT. He is currently on sabbatical leave and working at VTI Technologies.

Antti Lipsanen received his M.Sc. (Tech.) and Lic.Sc. (Tech.) degrees in electrical and communications engineering from Helsinki University of Technology, Finland in 2000 and 2004, respectively.

He is currently a Process Design Engineer at VTI Technologies Oy, Finland.

Aarne Oja received his Dr. Tech. degree in 1988 from the Low Temperature Laboratory of the Helsinki University of Technology. Before joining VTT at 1995 he investigated nuclear magnetism at nanokelvin temperatures. He is the leader of MEMS Sensors group at VTT Microsensing and Research Professor since 2000. His current research interests include several micro-electromechanical sensors and devices: RF-resonators, high-precision MEMS, ultrasound sensors, and magnetic MEMS.